A Study of Creeping Sinusoidal Flow of Bio-Rheological Fluids through a Two-Dimensional High Permeability Medium Channel

Dharmendra Tripathi[1,*], O. Anwar Bég[2], V.S. Pandey[3] and A.K. Singh[4]

[1]*Department of Mathematics, National Institute of Technology – Delhi, Dwarka, Sector – 9, Delhi 110077, India*

[2]*Gort Engovation Research (Aerospace Propulsion and Biomechanics), 15 Southmere Avenue, Great Horton, Bradford, BD7 3NU, West Yorkshire, UK*

[3]*Department of Physics, National Institute of Technology – Delhi, Dwarka, Sector – 9, Delhi 110077, India*

[4]*Department of Computer Science and Engineering, National Institute of Technology – Delhi, Dwarka, Sector – 9, Delhi 110077, India*

Abstract: The creeping sinusoidal flow of non-Newtonian couple stress fluids in a two-dimensional porous medium channel with deformable walls, is investigated as a model of peristaltic physiological gastric transport. A mathematical model is developed which is also applicable to hemodynamics of diseased arteries. The assumptions of long wavelength and low Reynolds number approximation are employed for creeping (viscous-dominated) flow. Solutions for axial velocity, volumetric flow rate, pressure gradient and stream function are obtained. The influence of couple stress rheological parameter and permeability parameter on velocity profile, pressure gradient and stream lines patterns are computed with the aid of **Mathematica** Software.

Keywords: Sinusoidal wave propagation, Couple stress fluid, Porous channel, Stream lines, Cerebral diseased hemodynamics, Gastric flow.

1. INTRODUCTION

Peristaltic flow arises in numerous physiological systems and constitutes an example of *fluid-structure interaction* [1]. Associated with rhythmic transport and deformable conduits, peristaltic flows are generically transient in nature and propagate in deformable geometrical configurations. They frequently exhibit a sinusoidal creeping flow as exemplified by migration of gastric fluids (bolus) through the oesophagus and human stomach [2], motion of chyme through large and small intestines [3] etc. Classical mathematical modeling of peristaltic flows has been an active area of applied mathematics for over four decades. Pioneering studies in this regard include the creeping sinusoidal channel flow of Newtonian fluids in peristaltic transport as studied by Shapiro *et al.* [4], Fung *et al*. [5]. These analyses generally employ the *long wave length approximation* and some form of lubrication theory which allows the reduction of Navier-Stokes equations to Stokesian (creeping flow) equations, in which inertial terms are generally neglected. They also address either infinite conduits or finite length conduits but are nevertheless restricted to relatively simple geometries and Newtonian fluids. In recent years many theoretical and computational approaches have been developed to simulate peristaltic fluid-structure interaction (**FSI**) problems and these have aimed to achieve either more sophisticated geometric modeling and/or simulate more physically accurate biological liquid properties. Interesting studies of geometric complex fluid structure interaction flows include Crosetto *et al.* [6] who studied aortic FSI and Buriev *et al.* [7] who investigated stenotic blood FSI problems numerically. Quite recently an interesting study has been communicated on peristaltic FSI by Yazdanpanh-Ardakani and Niroomand-Oscuii [8] simulated unsteady rheological axisymmetric peristaltic transport with a finite element code, ADINA. Aboelkassem and Staples [9] considered peristaltic biomimetic pumping flows in a complex network of insect trachea in the microscale flow regime. As elaborated earlier these recent simulations of peristalsis have been confined to *Newtonian fluids* or in the case of [10] to very elementary rheological models. The complex rheology of real biological fluids however requires more sophisticated mathematical models capable of capturing the non-Newtonian characteristics of these liquids, which are generally suspensions. In recent years, therefore, a diverse array of rheological models, have been implemented in peristaltic transport modeling. These include Maxwell fluids [11], Jeffreys fluids [12], Williamson fluids [13], Oldroyd-B fluids [14], Johnson-Segalman fluids [15], nanofluids [16], liquid crystal nematogens [17] and viscoplastic (Bingham)

*Address correspondence to this author at the Department of Mathematics, National Institute of Technology – Delhi, Dwarka, Sector – 9, Delhi 110077, India; E-mails: dtripathi@nitdelhi.ac.in, dharmtri@gmail.com

E-ISSN: 2311-1755/13

yield stress fluids [18]. All these models involve a tremendous range of constitutive equations and mimick extensive features arising in actual rheological fluids. One particular model, the Stokes couple stress fluid [19] is a special sub-class of non-Newtonian fluids which allows for particle sizes to be taken into account. The classical Navier-Stokes (continuum) theory or generalized non-Newtonian models (viscoelastic, viscoplastic etc.) do not simulate particle size effects. To overcome this, a micro-continuum theory was presented by Stokes [20] which can capture particle size effects. The Stokes micro-continuum theory is a generalization of the classical theory of fluids allowing for polar effects such as the presence of couple stresses, body couples, and an anti-symmetric stress tensor. In this fluid model, the couple stress effects are considered as a consequence of the action of a deforming body on its neighborhood. The Stokes model has proven very popular in analyzing biological flows including lubrication (tribological) systems [21], microcirculation hemodynamics [22-28], centrifugal biomedical separation devices [29, 30]. Relatively few studies of peristaltic flows of couple stress fluids have been communicated. An early analysis has been presented by Srivastava [31]. Mekheimer [32] has also examined peristaltic flow of a couple stress fluids including magnetic induction effects.

In numerous gastric and circulation flows, debris may be deposited in biological conduits (arteries, intestines, veins, capillaries) and this is a manifestation of diseased systems. The normally homogenous flow regime therefore becomes a porous medium and can be simulated using models which evaluate the supplementary drag forces exerted on the flow due to the presence of solid matrix fibers. These fibers may be bacterial clumps, undigested components of food, clusters of fatty deposits in arteries etc. As such the viscosity of such regimes will also be affected [33, 34]. Small intestine partial blockages effectively impede the transit of oncoming chyme. The regime can be simulated *via* a *porous medium drag force model*, as emphasized by Khaled and Vafai [35]. An important disease which shows impedance features is Hirschsprung's disease - a congenital disorder in which poor motility which induces obstruction of both the small and large intestines. In partial obstructions, some liquid chyme contents are able to pass through the obstruction zones, and this effectively can be modelled as a porous medium problem. The presence of infections (e.g. ulcers) leading to material deposition in the small intestine decelerates the propagation of waves and inhibits chyme migration. Effectively the purely fluid regime (healthy intestine) is transformed to a porous medium regime (diseased intestine). In hemodynamics, porous media drag force models are also a very useful tool for simulating impedance to circulation. Recently several simulations of couple stress biophysical peristaltic flows in porous media have been communicated, including the hemodynamic study by Tripathi [36] which includes hydrodynamic wall slip effects, and the gastric model examined by Tripathi and Bég [37]. Tripathi [38] has further considered collective wall slip and magnetic body force effects in couple stress peristaltic flow through porous media, showing analytically that pressure is suppressed with increasing magnitude of couple-stress parameter, permeability parameter and wall slip parameter, whereas it is elevated with stronger transverse magnetic field and amplitude ratio effects.

In the present study we consider for the first time, the peristaltic transport of non-Newtonian couple stress fluids in a two-dimensional sparse porous medium channel with deformable walls, under long wavelength and low Reynolds number approximations, valid for creeping (viscous-dominated) flow. Analytical solutions are derived for axial velocity, volumetric flow rate, pressure gradient and stream function. We elaborate on the effects of the couple stress rheological parameter and permeability (porous medium hydraulic conductivity) parameter on flow characteristics and also present visualizations of the stream lines patterns. The study is aimed at further investigating the hemodynamic transport in diseased gastric systems with more realistic rheological formulations. Weak blockages are simulated using high permeability values. **Mathematica** software is employed to *visualize peristaltic wave patterns* at various permeabilities and couple stress parameter values.

2. COUPLE STRESS RHEOLOGICAL EQUATIONS AND SINUSOIDAL FLOW MODEL

In this study we adopt the Stokesian couple stress rheological model [20]. Couple stresses are the generated based on the assumption that the mechanical action of one part of a body on another across a surface is Equivalent to a force and moment distribution. In the classical non-polar theory (Navier-Stokes viscous fluids), moment distributions are not considered and the mechanical action is assumed to be Equivalent to a force distribution only as elucidated by Cowin [39]. The state of stress is measured by a stress tensor τ_{ij} and a couple stress tensor, M_{ij}. The

tensorial form of the field Equations for Stokes couple stress fluids may be shown to take the form:

Mass Conservation (Continuity)

$$\dot{\rho} + \rho v_i = 0, \tag{1}$$

Cauchy's First Law of Motion

$$\rho a_i = T_{ji,j} + \rho f_i , \tag{2}$$

Cauchy's Second Law of Motion

$$M_{ji,j} + \rho l_i + e_{ijk} T_{jk} = 0, \tag{3}$$

Here ρ denotes the density of the couple stress fluid, v_i the velocity components, a_i are the components of the acceleration, T_{ij} is the second order stress tensor, M_{ij} the second order couple stress tensor, f_i the body force per unit volume, l_i the body moment per unit volume and e_{ijk} the third order alternating pseudo tensor, which is equal to +1 or −1 if (*i, j,k*) is an (even or odd) permutation of (1,2,3), and vanishes if two or more of the indices *i, j, k* are equal. For *incompressible couple stress fluids* and if the body force and body moment are absent, the equations of motion can be shown to reduce, in *vectorial notation*, to:

$$\rho a_i = -\nabla P + \nabla \cdot (\tau_{ij}) - \mu_1 \nabla^4 v \, . \tag{4}$$

Here $\boldsymbol{\tau}_{ij}$ is the stress tensor in the nonpolar classical theory [39] and μ_1 is the *couple stress coefficient*. The final term in Eqn. (4) represents the couple stresses. This constitutive Equation is utilized in due course.

The walls of channel are simulated as a sinusoidal wave propagating and the appropriate geometrical formulation, as depicted visually in Figure **1**, is defined as follows:

$$\tilde{h} = a + b \sin \frac{2\pi}{\lambda} (\tilde{\xi} - c\tilde{t}) , \tag{5}$$

where a, is the half width of the channel, b is amplitude, λ is wavelength, c is the wave velocity and $\tilde{t}$ is time.

3. TWO-DIMENSIONAL COUPLE STRESS POROUS MEDIUM FLOW MODEL

Neglecting the body forces and the body couples, the two-dimensional transient, continuity equation and equations of motion for couple stress fluid flow through porous medium, employing the relevant terms from Eqn. (4), take the form:

$$\frac{\partial \tilde{u}}{\partial \tilde{\xi}} + \frac{\partial \tilde{v}}{\partial \tilde{\eta}} = 0 , \tag{6}$$

$$\rho \left(\frac{\partial \tilde{u}}{\partial \tilde{t}} + \tilde{u} \frac{\partial \tilde{u}}{\partial \tilde{\xi}} + \tilde{v} \frac{\partial \tilde{u}}{\partial \tilde{\eta}} \right) = -\frac{\partial \tilde{p}}{\partial \tilde{\xi}} + \mu \nabla^2 \tilde{u} - \mu_1 \nabla^4 \tilde{u} - \frac{\tilde{u}}{\tilde{K}} , \tag{7}$$

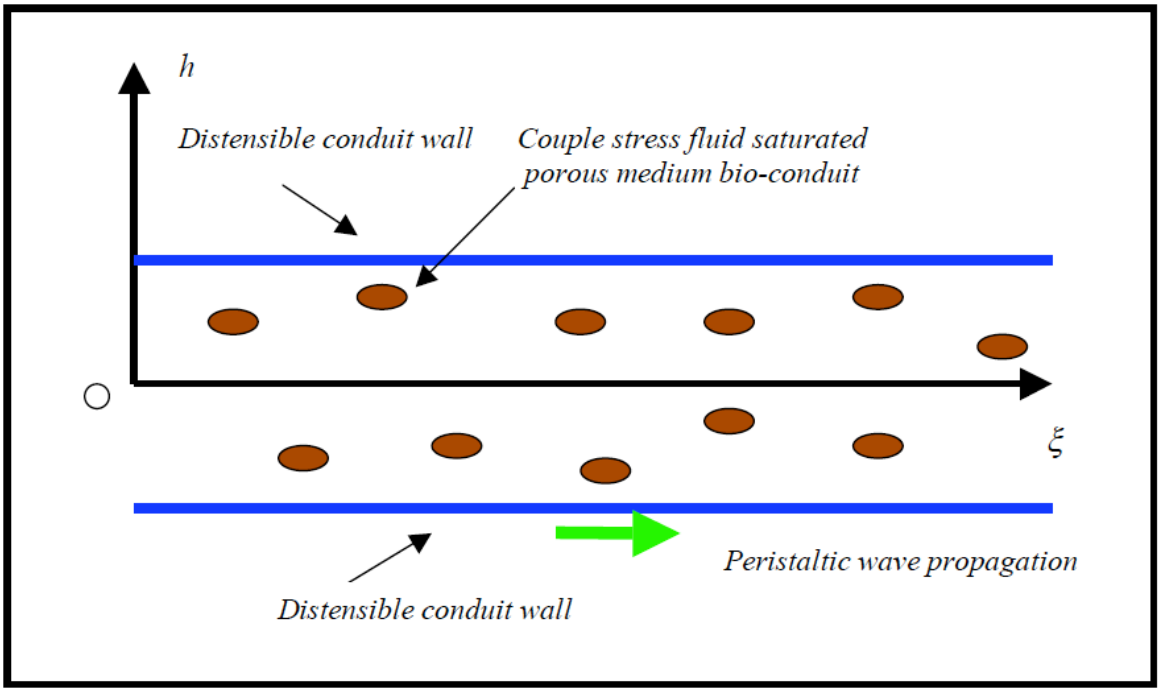

Figure 1: Geometry of sinusoidal channel flow regime.

$$\rho\left(\frac{\partial \tilde{u}}{\partial \tilde{t}}+\tilde{u}\frac{\partial \tilde{v}}{\partial \tilde{\xi}}+\tilde{v}\frac{\partial \tilde{v}}{\partial \tilde{\eta}}\right)=-\frac{\partial \tilde{p}}{\partial \tilde{\eta}}+\mu\nabla^2\tilde{v}-\mu_1\nabla^4\tilde{v}-\frac{\tilde{v}}{\tilde{K}}, \quad (8)$$

where $\rho,\tilde{u},\tilde{v},\tilde{\eta},\tilde{p},\mu,\mu_1,\tilde{K}$ are the couple stress fluid density, axial velocity, transverse velocity, transverse coordinate, pressure, dynamic viscosity, constant coefficient associated with couple stress and the permeability parameter, respectively, and the following Laplacian definition holds:

$$\nabla^2\equiv\frac{\partial^2}{\partial\tilde{\xi}^2}+\frac{\partial^2}{\partial\tilde{\eta}^2},\ \nabla^4=\nabla^2\nabla^2. \quad (9)$$

4. NON-DIMENSIONAL TRANSFORMATION AND ANALYTICAL SOLUTIONS

Introducing the following dimensionless parameters:

$$\left.\begin{aligned}&\xi=\frac{\tilde{\xi}}{\lambda},\ \eta=\frac{\tilde{\eta}}{a},\ u=\frac{\tilde{u}}{c},\ v=\frac{\tilde{v}}{c\delta},\ \phi=\frac{b}{a},\\&h=\frac{\tilde{h}}{a}=1+\phi\sin(2\pi(\xi-t)),\\&p=\frac{\tilde{p}a^2}{\mu c\lambda},\ K=\frac{\tilde{K}}{a^2},\ \mathrm{Re}=\frac{\rho ca}{\mu},\ \delta=\frac{a}{\lambda},\alpha=a\sqrt{\frac{\mu}{\mu_1}},\end{aligned}\right\} \quad (10)$$

where $\delta,\varepsilon,\phi,\mathrm{Re},\alpha$ are the wave number, ratio of half width of channels, amplitude ratio, Reynolds number and couple stress parameter respectively and applying the long wavelength and low Reynolds number approximation, in the framework of lubrication theory, in Eqns. (6)-(9), we obtain:

$$\frac{\partial u}{\partial\xi}+\frac{\partial v}{\partial\eta}=0, \quad (11)$$

$$\frac{\partial p}{\partial\xi}=\frac{\partial^2 u}{\partial\eta^2}-\frac{1}{\alpha^2}\frac{\partial^4 u}{\partial\eta^4}-\frac{u}{K}, \quad (12)$$

$$\frac{\partial p}{\partial\eta}=0. \quad (13)$$

The boundary conditions are:

no slip condition, $u=0\ at\ \eta=h$, *regularity condition*,

$$\frac{\partial u}{\partial\eta}=0\ at\ \eta=0, \quad (14)$$

vanishing of couple stresses, $\frac{\partial^2 u}{\partial\eta^2}=0\ at\ \eta=h$,

$$\frac{\partial^3 u}{\partial\eta^3}=0\ at\ \eta=0. \quad (15)$$

Solution of Eqn. (12), with boundary conditions (14) and (15), we arrive at:

$$u=K\frac{\partial p}{\partial\xi}\left[\frac{1}{(m_2^2-m_1^2)}\left\{\frac{m_2^2\cosh(m_1\eta)}{\cosh(m_1h)}-\frac{m_1^2\cosh(m_2\eta)}{\cosh(m_2h)}\right\}-1\right], \quad (16)$$

where

$$m_1=\sqrt{\frac{\alpha^2+\alpha\sqrt{\alpha^2-4/K}}{2}}, \quad (17)$$

$$m_2=\sqrt{\frac{\alpha^2-\alpha\sqrt{\alpha^2-4/K}}{2}}, \quad (18)$$

The volume flow rate is given by

$$Q=\int_0^h u d\eta. \quad (19)$$

Implementing Eqn. (16) in Eqn. (19) yields:

$$Q=K\frac{\partial p}{\partial\xi}\left[\frac{1}{(m_2^2-m_1^2)}\left\{\frac{m_2^2}{m_1}\tanh(m_1h)-\frac{m_1^2}{m_2}\tanh(m_2h)\right\}-h\right]. \quad (20)$$

The transformations between a wave frame $(\tilde{X},\tilde{Y})$ moving with velocity c and the fixed frame $(\tilde{\xi},\tilde{\eta})$ are defined thus:

$$\tilde{X}=\tilde{\xi}-c\tilde{t},\ \tilde{Y}=\tilde{\eta},\ \tilde{U}=\tilde{u}-c,\ \tilde{V}=\tilde{v}, \quad (21)$$

where $(\tilde{U},\tilde{V})$ and $(\tilde{u},\tilde{v})$ are the velocity components in the wave and fixed frame respectively.

The volumetric flow rate in fixed frame is given by:

$$Q=\int_0^h u d\eta=\int_0^h (U+1)dY, \quad (22)$$

which, on integration,

$$Q=q+h. \quad (23)$$

Averaging volumetric flow rate along one time period, gives:

$$\bar{Q}=\int_0^1 Q dt. \quad (24)$$

From Eqn. (23) & Eqn. (24) we have:

$$\bar{Q}=Q+1-h. \quad (25)$$

From Eqn. (20) and Eqn. (25), the pressure gradient is obtained as:

$$\frac{\partial p}{\partial \xi} = \frac{\bar{Q} - 1 + h}{K\, f(\xi)}, \tag{26}$$

where

$$f(\xi) = -h + \frac{1}{(m_2^2 - m_1^2)} \left\{ \frac{m_2^2}{m_1} \tanh(m_1 h) - \frac{m_1^2}{m_2} \tanh(m_2 h) \right\}. \tag{27}$$

From Eqn. (16) and Eqn. (26), and using the transformations defined in Eqn. (21), the *stream function in the wave frame* ($U = \frac{\partial \psi}{\partial \eta}$ and $V = -\frac{\partial \psi}{\partial \xi}$) assumes the form:

$$\psi(\xi, \eta) = \frac{\bar{Q} - 1 + h}{f(\xi)} \left[-\eta + \left\{ \frac{m_2^2 \sinh(m_1 \eta)}{m_1 \cosh(m_1 h)} - \frac{m_1^2 \sinh(m_2 \eta)}{m_2 \cosh(m_2 h)} \right\} \right] - \eta. \tag{28}$$

The results reduce to the classical Newtonian solutions obtained by Shapiro *et al.* [4] when $\alpha \to 0$ (vanishing couple stress effect) and $K \to \infty$ (infinite permeability i.e. purely fluid regime).

5. NUMERICAL COMPUTATIONS AND DISCUSSION

Computational results have been generated using **Mathematica** software for the influence of *permeability parameter* (*K*) and *couple stress parameter* (α), on flow characteristics, as illustrated in Figures **2-4**. *Mathematica* is a leading symbolic "computational library" [40] which has emerged as a very powerful numerical computational tool, with systemwide technology to ensure reliability, ease of use, and performance. *Mathematica* computation directly permits seamless workflow, unique symbolic language, and advanced code editing environment, achieving fast turnaround on small projects and record times on large systems. *Mathematica*'s 2D and 3D graphics are represented using symbolic primitives, and can therefore be generated and manipulated using all standard *Mathematica* functions and seamlessly integrated with text, math, or tables. With region- and volume-oriented implicit plotting, automated singularity analysis, arbitrary plotting regions and mesh overlays, and more, *Mathematica* enables the immediate creation of highly aesthetic and technically correct 2D and 3D visualizations. A comprehensive set of function

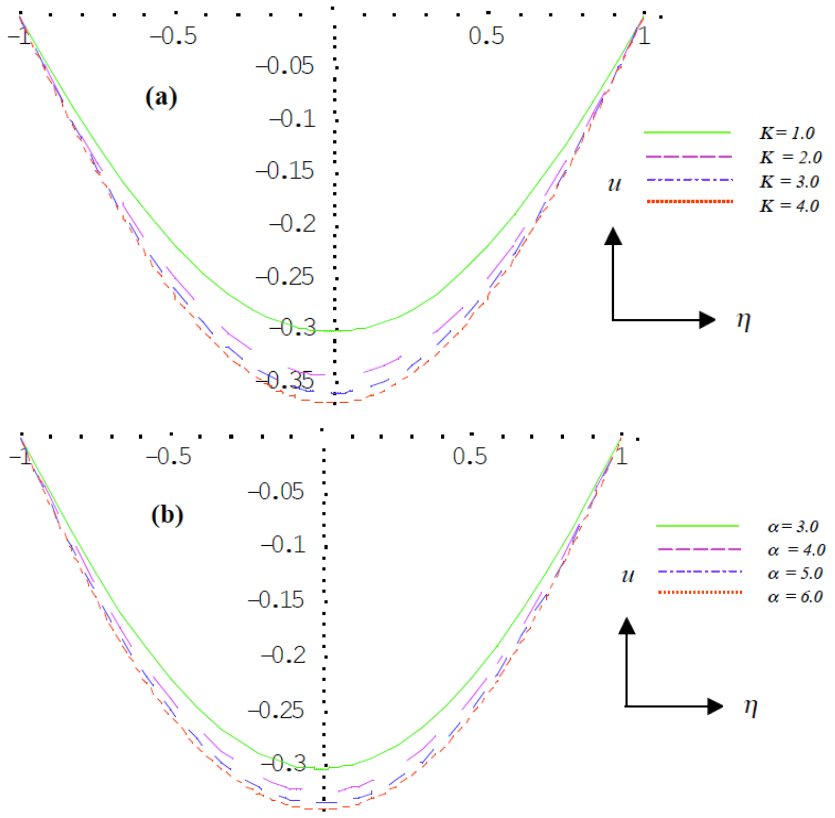

Figure 2: Velocity Profile (Axial velocity vs. Transverse displacement) at $\xi = 1, \phi = 0.5, t = 1.0, \frac{\partial p}{\partial \xi} = 1$ for different values of **(a)** $K = 1, 2, 3, 4$ **(b)** $\alpha = 3, 4, 5, 6$.

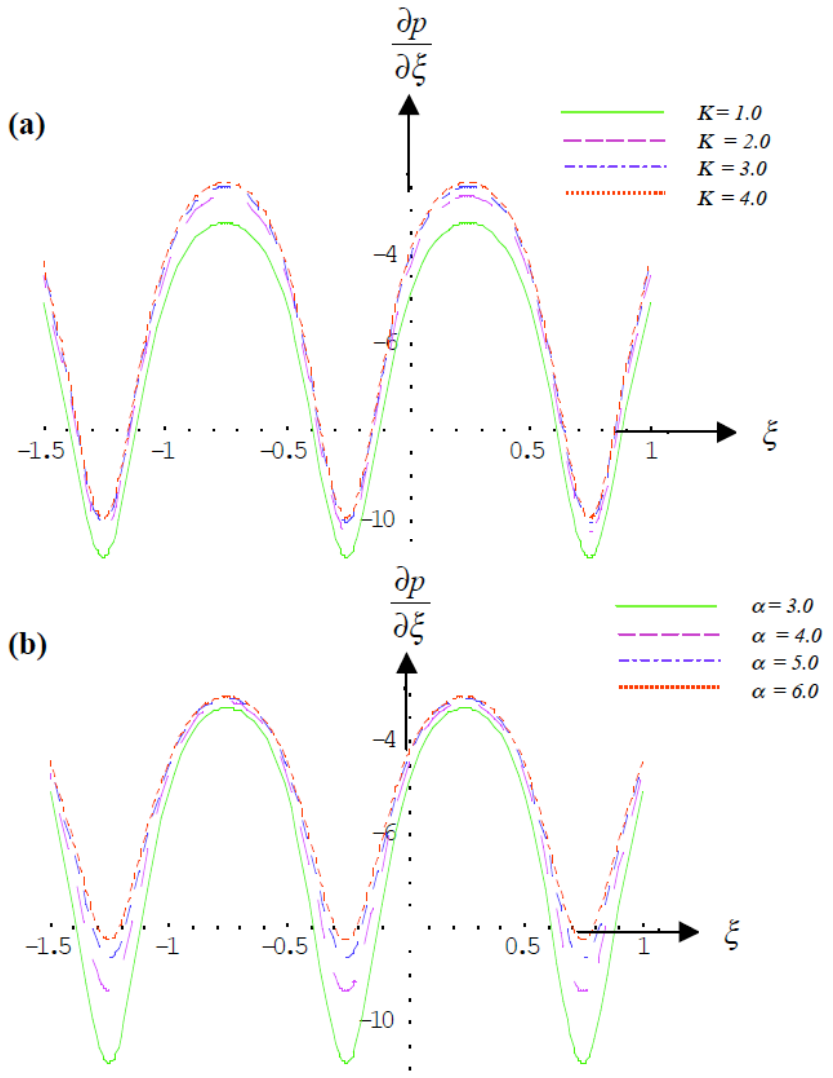

Figure 3: Pressure Gradient vs. Axial displacement at $\phi = 0.3$, $\bar{Q} = 1.0$ for different values of **(a)** $K = 1,2,3,4$ **(b)** $\alpha = 3,4,5,6$.

visualization types are built in, including polar and spherical plots, contour and density plots, parametric line and surface plots, and vector and stream plots. Mathematica provides an enormous set of mathematical, scientific, engineering (and financial) functions which is easily accessible. However, *Mathematica* functions work for any size or precision of number, compute with symbols, are easily represented graphically, automatically switch algorithms to get the best answer, and even check and adjust the accuracy of their own results. This sophistication means great dependability and confidence in solutions, especially for engineering-type mathematical calculations. *Mathematica*'s symbolic architecture allows both equations and their solutions to be conveniently given in symbolic form, and immediately integrated into computations and visualizations. Automatically selecting between hundreds of powerful and in many cases original algorithms, *Mathematica* provides both numerical and symbolic solving of differential equations (ODEs, PDEs etc). With equations conveniently specified symbolically, *Mathematica* uses both its rich set of special functions and its unique symbolic interpolating functions to represent solutions in forms that can immediately be manipulated or visualized [40]. All the results for *axial velocity* (Eqn.16), *volumetric flow rate* (Eqn.21), *pressure gradient* (Eqn.26) and *stream function* (Eqn.28) have been obtained in the form of two arbitrary functions, $m_1\left(=\sqrt{\frac{\alpha^2+\alpha\sqrt{\alpha^2-4N}}{2}}\right)$ and $m_2\left(=\sqrt{\frac{\alpha^2-\alpha\sqrt{\alpha^2-4N}}{2}}\right)$, which depend on couple stress parameter (α) and permeability parameter (K). All the computations have been performed for real values of m_1 and m_2 i.e. $\alpha^2 > 4/K$.

Figure **2a** & **b** depict the effects of couple stress parameter (α) and permeability parameter (K) on velocity profile (axial velocity vs. transvers displacement) at a fixed value of axial displacement,

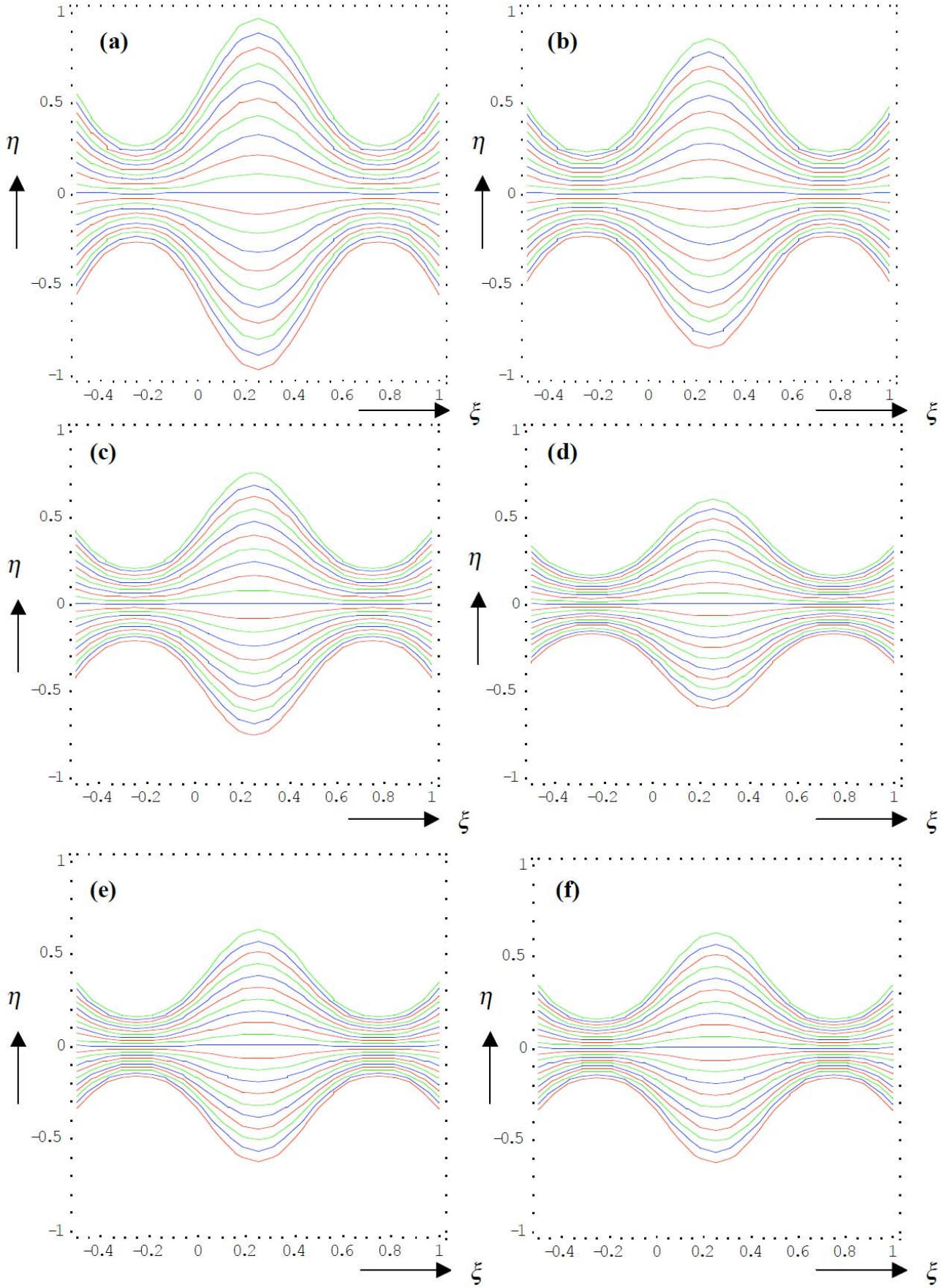
(a)
(b)
(c)
(d)
(e)
(f)
η
ξ
1
0.5
0
−0.5
−1
−0.4
−0.2
0
0.2
0.4
0.6
0.8
1

(Figure 4). Continued.

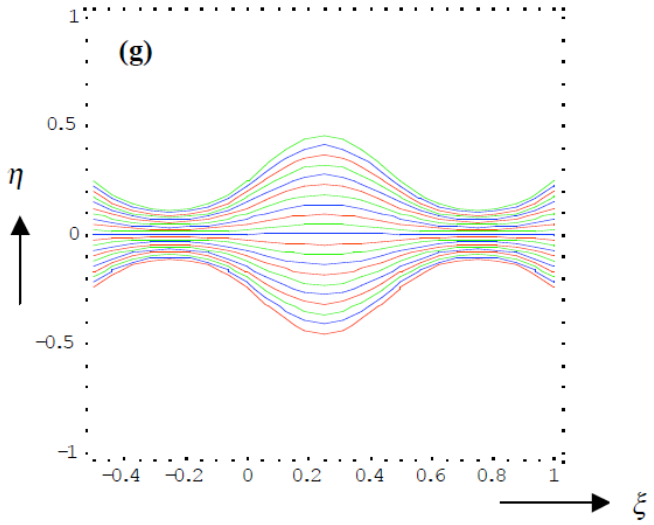

Figure 4: Streamlines in the wave frame at $\bar{Q}=0.6,\ \phi=0.6$ for

(a) $K=1,\ \alpha=3$,

(b) $K=1,\ \alpha=3.25$,

(c) $K=1,\ \alpha=3.5$,

(d) $K=1,\ \alpha=4$,

(e) $K=1.25,\ \alpha=3$,

(f) $K=1.5,\ \alpha=3$,

(g) $K=2,\ \alpha=3$.

amplitude ratio, time, and pressure gradient (i.e., $\xi=1,\ \phi=0.5,\ t=1.0,\ \frac{\partial p}{\partial \xi}=1$). The profiles are parabolic which correlate well with the classical Newtonian viscous creeping flow solutions of Shapiro *et al.* [4]. Figure **2a** depicts the effect of couple stress parameter (α) on velocity profile and it is found that axial velocity in magnitude *increases* with increase the magnitude of couple stress parameter.

The effect of permeability parameter (K) on velocity profile is similar to that of the couple stress parameter. An increase in *K* decreases proportionally the Darcian linear drag force appearing in the axial momentum conservation Eqn. (12), viz, $-\frac{u}{K}$. Effectively as the concentration of debris decreases in the bio-conduit, progressively less and less solid particles are present. The permeability of the regime is therefore increased and simultaneously the impedance force acting on the percolating couple stress fluid is decreased. This serves to *accelerate* the axial peristaltic creeping flow magnitudes. The negative signs indicate that the flow actually is directed in the opposite direction to the propagation of the peristaltic wave i.e. in the negative ξ-direction. The increase in the couple stress parameter also induces a significant decrease in the couple stress term, $-\frac{1}{\alpha^2}\frac{\partial^4 u}{\partial \eta^4}$. This term also acts like a supplementary drag force. Therefore the inverse square proportionality between the entire couple stress term and the couple stress coefficient,α, clearly implies that larger α values will lead to massively reduced magnitudes in $1/\alpha^2$, and this will effectively accelerate the axial flow. It is interesting to note however that the order of magnitude of axial velocity is similar for both the permeability effect and the couple stress effect. The enhancement in flow acceleration (albeit in the negative axial direction) has also been computed with high couple stress parameter effects by numerous other researchers including Sinha and Singh [22], Zueco and Bég [26], Srivastava [28] and Mekheimer [32].

Figure **3a** & **b** show the relationship between pressure gradient and axial displacement for a prescribed volumetric flow rate and amplitude ratio (i.e., $\phi=0.3,\ \bar{Q}=1.0$) with different values of couple stress parameter and permeability parameter. The curves exhibit periodicity with period of 0.5 (axial displacement) and are strongly nonlinear. Figure **3a** shows that the pressure gradient is markedly elevated

with increasing magnitude of couple stress parameter. Increasing rheological effects therefore require greater pressure for propagation of the peristaltic wave. A similar pattern is observed in Figure **3b** for the effect of permeability parameter on pressure gradient. In both cases, peak and trough amplitudes are enhanced with increasing couple stress or permeability effects.

Figure **4a-g** finally illustrate the stream line patters for the sinusoidal wavy channel flow for different values of couple stress parameter and permeability parameter, at fixed volumetric flow rate and amplitude ratio (i.e., $\bar{Q} = 0.6, \phi = 0.6$). Figure **4a-g** show that the stream line patterns are clearly of a sinusoidal wavy nature. From Figure **4a-d**, it is shown that the distance between two successive stream lines reduces with increasing the magnitude of couple stress parameter. From Figure **4e-g**, similar effects for the permeability parameter on stream line pattern are observed. Bolus magnitude is clearly decreased with increasing couple stress parameter and permeability effect. The deviations from Newtonian purely fluid flow are considerable and indicate that particle effects in real biological flows exert a non-trivial influence on peristaltic flows.

6. CONCLUSIONS

The two dimensional sinusoidal wavy motion of couple stress fluids through a deformable channel containing a sparsely packed porous medium has been analyzed. **Mathematica** visualizations of the analytical solutions for the resulting boundary value problem have shown that:

- Axial velocity magnitude increases with a rise in magnitude of couple stress parameter and also with permeability parameter (K).
- Pressure gradient is elevated with an increase in both couple stress and permeability parameters.
- Successive stream lines narrow with increasing magnitude of couple stress parameter and also with permeability parameter.
- Bolus size is depressed with increasing couple stress or permeability effects.

The present computations constitute a first step in simulating peristaltic flow of non-Newtonian fluids in distensible channels. Future investigations will employ commercial CFD codes to increase geometrical sophistication and peristaltic flow in *curved* geometries [41] ("non-Newtonian Dean flows") and will be communicated imminently.

REFERENCES

[1] Bathe KJ, Ledezma GA. Benchmark problems for incompressible fluid flows with structural interactions. Comput Struct 2007; 85: 628-44. http://dx.doi.org/10.1016/j.compstruc.2007.01.025

[2] Ferrua MJ, Singh RP. Modeling the fluid dynamics in a human stomach to gain insight of food digestion. Food Sci 2010; 75: R151-62. http://dx.doi.org/10.1111/j.1750-3841.2010.01748.x

[3] Tripathi D, Pandey SK, Bég OA. Mathematical modelling of heat transfer effects on swallowing dynamics of viscoelastic food bolus through the human oesophagus. Int J Thermal Sci 2013; 70: 41-53. http://dx.doi.org/10.1016/j.ijthermalsci.2013.03.005

[4] Shapiro AH, Jafferin MY, Weinberg SL. Peristaltic pumping with long wavelengths at low Reynolds number. J Fluid Mech 1969; 37: 799-825. http://dx.doi.org/10.1017/S0022112069000899

[5] Fung YG, Yih CS. Peristaltic transport. ASME: J Appl Mech 1968; 35: 669-75.

[6] Crosetto P, Reymond P, Deparis S, Kontaxakis D, Stergiopulos N, Quarteroni A. Fluid structure interaction simulations of physiological blood flow in the aorta. Computers Fluids 2011; 43: 46-57. http://dx.doi.org/10.1016/j.compfluid.2010.11.032

[7] Buriev B, Kim T, Seo T. Fluid-structure interactions of physiological flow in stenosed artery. Korea-Australia Rheology J 2009; 21: 39-46.

[8] Yazdanpanh-Ardakani K, Niroomand-Oscuii H. New approach in modeling peristaltic transport of non-Newtonian fluid. J Mech Med Biol 2013; 13: 1350052.1-1350052.14.

[9] Aboelkassem Y, Staples AE. Selective pumping in a network: insect-style microscale flow transport. Bioinspir Biomim 2013; 8: 026004. http://dx.doi.org/10.1088/1748-3182/8/2/026004

[10] Hung TK, Brown TD. Solid particle motion in two-dimensional peristaltic flows. J Fluid Mech 1976; 73: 77-97. http://dx.doi.org/10.1017/S0022112076001262

[11] Tripathi D, Bég OA. A numerical study of oscillating peristaltic flow of generalized Maxwell viscoelastic fluids through a porous medium. Trans Porous Med 2013; 95: 337-48. http://dx.doi.org/10.1007/s11242-012-0046-5

[12] Bég OA, Elsayed AF, Alarabi T. Cross-diffusion effects on variable-property viscoelastic peristaltic flow in an eccentric cylinder with curved compliant walls: homotopy perturbation method study. Comp Biol Med 2013; in press.

[13] Bég OA, Keimanesh M, Rashidi MM, Davoodi M. Multi-step DTM simulation of magneto-peristaltic flow of a conducting Williamson viscoelastic fluid. Int J Appl Math Mech 2013; 9: 1-19.

[14] Tripathi D, Bég OA, Curiel-Sosa JL. Peristaltic flow of generalized Oldroyd-B fluids with slip effects. Comput Methods Biomech Biomed Eng 2012. http://dx.doi.org/10.1080/10255842.2012.688109

[15] Hina S, Hayat T, Alsaedi A. Heat and mass transfer effects on the peristaltic flow of Johnson-Segalman fluid in a curved channel with complaint walls. Int J Heat Mass Tran 2012; 55: 3511-21. http://dx.doi.org/10.1016/j.ijheatmasstransfer.2012.03.014

[16] Bég OA, Tripathi D. Mathematical simulation of peristaltic pumping with double-diffusive convection in nanofluids: a bio-nanoengineering model. Proc IMech E Part N: J Nanoeng Nanosys 2012; 225: 99-114.

[17] Cuennet JG, Vasdekis AE, De Sio L, Psaltis D. Optofluidic modulator based on peristaltic nematogen microflows. Nature Photonics 2011; 5: Pages: 234-8.

[18] Tripathi D, Bég OA. Mathematical modeling of peristaltic pumping of viscoplastic bio-fluids. Proc IMechE Part H: J Eng Med 2014; 228: 67-88.

[19] Stokes VK. Theories of fluid with micro-structure, Springer-Verlag, New York 1984. http://dx.doi.org/10.1007/978-3-642-82351-0

[20] Stokes, VK. Couple stress fluids. Phys Fluid 1966; 9: 1709-15. http://dx.doi.org/10.1063/1.1761925

[21] Yousif AE, Al-Allaq AA. The hydrodynamic squeeze film lubrication of the ankle joint. Int J Mech Eng Appl 2013; 1: 34-42.

[22] Sinha P, Singh C. Effects of couple stresses on blood flow through an artery with mild stenosis. Biorheology 1984; 21: 303-15.

[23] Pal D, Rudraiah N, Devanathan R. A couple stress model of blood flow in the microcirculation. Bull Math Biol 1988; 50: 329-44.

[24] Chaturani P, Upadhya VS. Pulsatile flow of a couple stress fluids through circular tubes with application to blood flow. Biorheology 1978; 15: 193-201.

[25] Chaturani P, Rathod PV. A critical study of Poiseuille flow of couple stress fluid with applications to blood flow. Biorheology 1981; 18: 235-44.

[26] Zueco J, Bég OA. Network numerical simulation applied to pulsatile non-Newtonian flow through a channel with couple stress and wall mass flux effects. Int J Appl Math Mech 2009; 5: 1-16.

[27] Valanis KC, Sun CT. Poiseuille flow of fluid with couple stress with applications to blood flow. Biorheology 1969; 6: 85-97.

[28] Srivastava VP. Flow of a couple stress fluid representing blood through stenotic vessels with a peripheral layer. Indian J Pure Appl Math 2003; 34: 1727-40.

[29] Bég OA, Ghosh SK, Ahmed S, Bég TA. Mathematical modeling of oscillatory magneto-convection of a couple-stress biofluid in an inclined rotating channel. J Mech Med Biol 2012; 12: 1-35. http://dx.doi.org/10.1142/S0219519411004654

[30] Ramana Murthy JV, Muthu P, Nagaraju G. Finite difference solution for MHD flow of couple stress fluid between two concentric rotating cylinders with porous lining. Int J Appl Math Mech 2010; 6: 1-28.

[31] Srivastava LM. Peristaltic transport of a couple stress fluid. Rheologica Acta 1986; 25: 638-41. http://dx.doi.org/10.1007/BF01358172

[32] Mekheimer KS. Effect of the induced magnetic field on the peristaltic flow of a couple stress fluid. Phys Lett A 2008; 372: 4271-8. http://dx.doi.org/10.1016/j.physleta.2008.03.059

[33] Kulaylat MN, Doerr RJ. Small bowel obstruction, Surgical Treatment: Evidence-Based and Problem-Orientated, Holzheimer RG, Mannick JA, Eds. Munich, Zuckschwerdt Publishers 2011.

[34] Takeuchi K, Satoh H. Measurement of small intestinal damage. Curr Protoc Toxicol 2010; 45: 21.7.1-21.7.31.

[35] Khaled ARA, Vafai K. The role of porous media in modelling flow and heat transfer in biological tissues. Int J Heat Mass Transfer 2003; 24: 195-203.

[36] Tripathi D. Peristaltic hemodynamic flow of couple-stress fluids through a porous medium with slip effect. Trans Porous Med 2012; 92: 559-72. http://dx.doi.org/10.1007/s11242-011-9920-9

[37] Tripathi D, Bég OA. Magnetohydrodynamic peristaltic flow of a couple stress fluid through coaxial channels containing a porous medium. J Mech Med Biol 2012; 12: 1250088.1-1250088.20.

[38] Tripathi D. Peristaltic flow of couple-stress conducting fluids through a porous channel: applications to blood flow in the micro-circulatory system. J Biol Syst 2011; 19: 461. http://dx.doi.org/10.1142/S021833901100407X

[39] Cowin SC. Polar fluids. Phys Fluids 1968; 11: 1919-27. http://dx.doi.org/10.1063/1.1692219

[40] Wolfram. The Mathematica Book, Cambridge University Press, UK 1999; p. 1470.

[41] Norouzi M, Davoodi M, Bég OA, Joneidi AA. Analysis of the effect of normal stress differences on heat transfer in creeping viscoelastic Dean flow. Int J Thermal Sci 2013; 69: 61-9. http://dx.doi.org/10.1016/j.ijthermalsci.2013.02.002

Received on 15-10-2013 Accepted on 22-11-2013 Published on 10-02-2014

DOI: http://dx.doi.org/10.12970/2311-1755.2013.01.02.2